SUPPLEMENTARY MATERIAL

Mutual independence of T_c and superfluid density under pressure in optimally-doped $LaFeAsO_{1-x}F_x$

G. Prando,[1,*] Th. Hartmann,[2] W. Schottenhamel,[1] Z. Guguchia,[3] S. Sanna,[4] F. Ahn,[2] I. Nekrasov,[5] C. F. B. Blum,[1] A. U. B. Wolter,[1] S. Wurmehl,[1,6] R. Khasanov,[3] I. Eremin,[2] and B. Büchner[1,6]

[1] *Leibniz-Institut für Festkörper- und Werkstoffforschung (IFW) Dresden, D-01171 Dresden, Germany*
[2] *Institut für Theoretische Physik III, Ruhr-Universität Bochum, D-44801 Bochum, Germany*
[3] *Laboratory for Muon Spin Spectroscopy, Paul Scherrer Institut, CH-5232 Villigen PSI, Switzerland*
[4] *Dipartimento di Fisica and Unità CNISM di Pavia, Università di Pavia, I-27100 Pavia, Italy*
[5] *Institute for Electrophysics, Russian Academy of Sciences, Ural Branch, Amundsen str. 106, Ekaterinburg, 620016, Russian Federation*
[6] *Institut für Festkörperphysik, Technische Universität Dresden, D-01062 Dresden, Germany*

(Dated: April 7, 2015)

PACS numbers: 74.70.Xa, 76.75.+i, 74.62.Fj, 74.20.Pq, 74.20.Rp

I. SYNTHESIS AND CHARACTERIZATION OF THE SAMPLES

The investigated polycrystalline $LaFeAsO_{1-x}F_x$ sample has been prepared using a two-step solid-state reaction similarly to what is described in Ref. 1. In the first step, LaAs was prepared from La lumps (Chempur, 99.9%) and As lumps (Chempur, 99.999%) reacting a stoichiometric ratio in an evacuated quartz tube placed in a two-zone furnace. In the second step, we used the resulting LaAs and mixed it with Fe (Alfa Aesar, 99.998%), Fe_2O_3 (Chempur, 99.999%), and FeF_3 (Alfa Aesar, 97%) in a stoichiometric ratio. All starting materials were homogenized by grinding in a ball mill. The resulting powder was pressed into pellets under Ar atmosphere using a pressure of 20 kN, and subsequently annealed in an evacuated quartz tube in a two-step annealing process at 940°C for 8 h and at 1150°C for 48 h.

The structural characterization of the obtained polycrystalline sample was performed by means of powder x-ray diffraction (XRD) on a Huber Guinier camera (Co K_α radiation). $LaFeAsO_{1-x}F_x$ is reported to crystallize in a tetragonal structure with space group $I4/m$ (No. 87).[2] All the reflections observed in our powder XRD data are consistently indexed with this structure (Fig. 1). Lattice constants $a = 4.0363$ Å and $c = 8.7298$ Å are estimated.

The microstructure and composition of the sample were examined by scanning electron microscopy (XL30 Philipps, IN400) equipped with an electron microprobe analyzer for semi-quantitative elemental analysis using the wavelength dispersive x-ray mode. We yield a F content of $x = 0.13$, corroborating that the current $LaFeAsO_{1-x}F_x$ sample is optimally doped in agreement with the critical temperature observed by dc magnetometry.

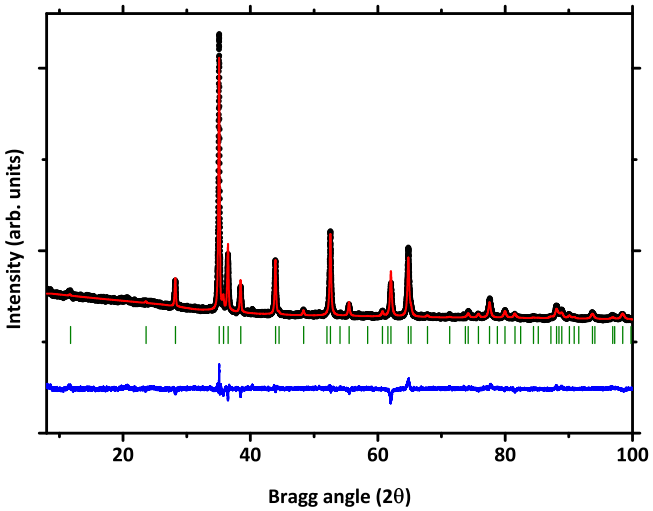

FIG. 1: Experimental data (black dots), simulated intensities (red line), Bragg positions (green bars) and the residual intensity (blue line) of XRD data taken on the investigated $LaFeAsO_{1-x}F_x$ sample.

II. MUON-SPIN SPECTROSCOPY (μ^+SR)

Measurements of zero- and transverse-field (ZF and TF, respectively) μ^+SR were performed at the Paul Scherrer Institute on the GPS and GPD spectrometers (πM3 and μE1 beamlines, respectively) for 1.6 K $< T <$ 200 K. In a μ^+SR experiment, a beam of spin-polarized positive muons μ^+ is implanted in well-defined crystallographic sites of the investigated material.[3,4] The time (t) dependence of the spin (de)polarization of μ^+, $P_T(t) = A_T(t)/A_0$, can be monitored as a function of temperature (T) and, accordingly, detailed information can be achieved about the local magnetic features characteristic of the material. Here, $A_T(t)$ is the so-called asymmetry function (see below) while A_0 is an experimental instrument-dependent parameter. In the case of superconductors, TF-μ^+SR is one of the most suited techniques in order to directly quantify the penetration length λ and, for single-crystalline and high-purity samples, to investigate the symmetry of the superconducting gap in detail.[3–10] Differently from, e. g., inductive techniques, TF-μ^+SR has then the great advantage of allowing one to properly achieve the absolute value of λ and not only its variations.

Data obtained in the low-background spectrometer GPS are used as reference for the more subtle analysis performed on data under P in the spectrometer GPD (see the data comparison in Fig. 2 later on). For measurements in GPD, the sample is inserted into a double-wall pressure cell (PC) made up of MP35N alloy. P is triggered by pistons of MP35N alloy, while the transmitting medium is Daphne oil 7373, ensuring almost-optimal conditions of hydrostaticity up to $P \sim 2$ GPa.[12,13] The actual value of P is measured at low-T by checking the superconducting transition temperature of a small indium manometer inside the cell by means of ac susceptibility. The ratio of incoming μ^+ implanted into the sample vs. incoming μ^+ implanted into the PC is $\sim$ 35 %. For this reason, it is crucial to characterize the magnetic behaviour of the cell in a separate set of TF-μ^+SR measurements in the same experimental conditions. In the case of superconducting materials for $T < T_c$, a stray magnetic field is induced outside the sample when an external field is applied. Accordingly, also μ^+ implanted into the PC and close enough to the sample will probe a distribution $P(B_\mu)$ of local magnetic field resulting in a corresponding damping of the relative TF-μ^+SR signal. The typical fitting function employed in order to analyse data is written as[14]

$$\frac{A_T^{\mathrm{TF}}(t)}{A_0} = a_s \exp\left[-\frac{\left(\sigma_n^2+\sigma_{sc}^2\right)t^2}{2}\right]\cos\left(\gamma B_\mu t+\phi\right) + (1-a_s)\exp\left[-\left(\frac{\sigma_{PC}^2 t^2}{2}+\lambda_{PC}t\right)\right]\times\int P(B'_\mu)\cos\left(\gamma B'_\mu t+\phi\right)dB'_\mu. \quad (1)$$

The parameter a_s is introduced in order to quantify the fraction of μ^+ implanted into the sample [specular to $(1-a_s)$ which accounts for μ^+ implanted into the PC], while B_μ quantifies the local magnetic field probed by μ^+ (the resulting oscillation is phase-shifted by the factor ϕ while $\gamma = 2\pi \times 135.54$ MHz/T represents the gyromagnetic ratio of μ^+). The T-independent Gaussian relaxation rate σ_n accounts for nuclear magnetism in the sample, while the T-dependent

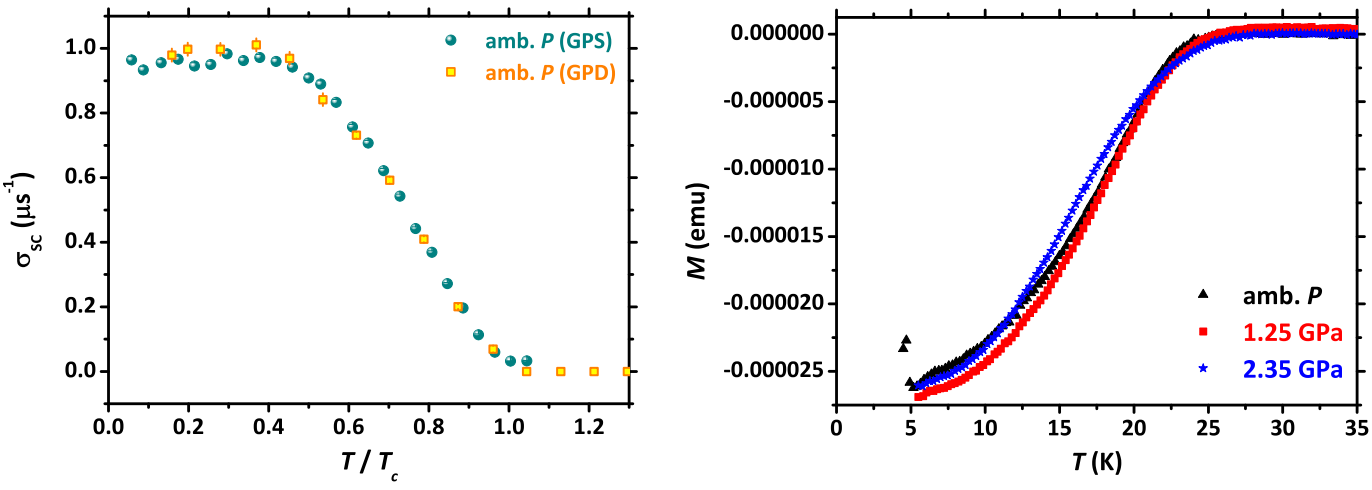

FIG. 2: Left panel: comparison of σ_{sc} data at ambient pressure as obtained in the low-background spectrometer GPS (without pressure cell) and in the spectrometer GPD with the sample loaded in the pressure cell. Right panel: FC magnetization of the investigated sample at $H = 600$ Oe for different P values within the experimental range of interest (after subtraction of the background contribution from the pressure cell).

Gaussian contribution σ_{sc} is the main outcome of the experiment, namely the extra-damping induced by the vortices. The relaxation rates σ_{PC} and λ_{PC} describe the intrinsic magnetic properties of the PC, where the distribution $P(B_\mu)$ is induced by the stray magnetic field from the sample. The actual shape of $P(B_\mu)$ is chosen in order to maximize the agreement between GPS and GPD data (ambient pressure). In the current case, $P(B_\mu)$ is such that 2/3 of the pressure cell ("inner shell", close to sample) feels a magnetic field equally distant from the magnetic field inside the sample (B_μ) and the externally applied field H_e (the precise value of this latter quantity being estimated for $T > T_c$) while the remaining 1/3 of the pressure cell ("outer shell", far from the sample) feels a magnetic field equal to the externally applied field H_e. Results of the comparison between GPS and GPD data are shown in Fig. 2 (left panel), where an excellent agreement can be observed. The actual shape of $P(B_\mu)$ is kept constant at all P values. This latter approximation is substantiated by measurements of the field-cooled magnetization of the sample at $H_e = 600$ Oe, namely, in the same conditions of the μ^+SR experiment (see the right panel of Fig. 2). The magnetization is indeed unchanged with increasing P, suggesting that the influence on the pressure cell should be similar and giving some independent strong ground to the assumption of independence of $P(B_\mu)$ on pressure.

The actual value of the external TF was chosen after performing a H-scan at $T = 1.6$ K aiming at maximizing the value of σ_{SC}. The overall σ_{SC} vs. H trend is in excellent quantitative agreement with previously reported data.[11] Accordingly, the value $H = 600$ Oe was selected for the T scans, both in GPS and in GPD.

III. DC MAGNETIZATION

The diamagnetic response of the sample was carefully studied by means of dc magnetometry in zero-field cooling (ZFC) conditions and upon the application of P. In particular, as discussed in the paper, the following information was extracted about superconductivity, namely T_c, transition width and superconducting shielding fraction. Measurements were performed in a commercial superconducting quantum interference device (SQUID) magnetometer MPMS-XL5 (Quantum Design). A homemade PC was employed, whose design is similar to that of a diamond anvil cell. Two opposing cone-shaped ceramic anvils compress a gasket with a small hole that serves as a sample chamber.[15] The applied uniaxial pressure onto the gasket is transformed into hydrostatic pressure in the sample chamber by using Daphne oil 7373 as transmitting medium. A single powder-grain is used as a sample. The actual P value is measured by monitoring the superconducting transition temperature of a small Pb manometer inside the sample chamber. All the mechanical parts are made of weakly-magnetic materials allowing a dramatic reduction of the background signal even in the (current) case of samples with tiny dimensions.

IV. NON-MAGNETIC IMPURITY SCATTERING IN A $s^{\pm}$ SUPERCONDUCTOR

Here, we present the derivation of the superconducting gap equations for the $s^{\pm}$ superconductor in presence of non-magnetic impurities, following Ref. 16. Here, the superconducting gaps are formed on the electron and on the hole bands of similar magnitudes but of opposite signs. In addition, the electron pockets are located around the $(\pi, 0)$ points of the BZ, which have lower symmetry than the Γ-point or the $M = (\pi, \pi)$ points of the BZ, where hole pockets are located. As a result, one should allow the $\cos 2\theta$ modulation of the gap on the electron pocket. Due to internal sign change of the gap between the electron and the hole pockets the effect of the non-magnetic impurity can be separated into the scattering within either hole and/or electron pockets (denoted as Γ_0), which does not influence the superconducting gap and T_c and the scattering between electron and hole pockets (here Γ_π), which behaves as magnetic impurity in this case with strong pair-breaking effects.

To find the gap equations we write the first two *Gorkov equations* for the hole and the electron pockets

$$\begin{aligned}
&[i\omega_m + \Gamma_0\bar{G}_h + \Gamma_\pi\bar{G}_e - \xi_h]G_h \quad + [\Delta_h + \Gamma_0\bar{F}_h + \Gamma_\pi\bar{F}_e]F_h^\dagger = 1,\\
&[i\omega_m + \Gamma_0\bar{G}_e + \Gamma_\pi\bar{G}_h - \xi_e]G_e + [\Delta_e(\theta) + \Gamma_0\bar{F}_e + \Gamma_\pi\bar{F}_h]F_e^\dagger = 1
\end{aligned} \tag{2}$$

where

$$\begin{aligned}
G_h = G_h(\tilde{\Delta}_m^h, \tilde{\omega}_m^h), \quad F_h = F_h(\tilde{\Delta}_m^h, \tilde{\omega}_m^h),\\
G_e = G_e(\tilde{\Delta}_m^e, \tilde{\omega}_m^e), \quad F_e = F_e(\tilde{\Delta}_m^e, \tilde{\omega}_m^e)
\end{aligned}$$

are the normal and the anomalous Green's function for the hole and the electron pockets, and $\bar{G}_h$ and $\bar{G}_e$ satisfy the

equations

$$\bar{G}_h = \frac{1}{\pi}\int d\xi_h G_h,$$
$$\bar{G}_e = \frac{1}{\pi}\int d\xi_e G_e.$$

In this model, the ansatz for the $s^{\pm}$-wave gap is

$$\Delta_e(\theta) = \Delta_e \pm \Delta_{\bar{e}}\cos(2\theta) \tag{3}$$

and $\Delta_h = -\Delta_e$. In the presence of impurities one defines the new Matsubara frequencies,

$$\begin{aligned} i\tilde{\omega}_m^h &= i\omega_m\eta_m^h = i\omega_m + \Gamma_0\bar{G}_h + \Gamma_\pi\bar{G}_e, \\ i\tilde{\omega}_m^e &= i\omega_m\eta_m^e = i\omega_m + \Gamma_0\bar{G}_e + \Gamma_\pi\bar{G}_h, \end{aligned} \tag{4}$$

as well as the superconducting gaps

$$\begin{aligned} \tilde{\Delta}_m^h &= \bar{\Delta}_m^h\eta_m^h \quad = \Delta_h + \Gamma_0\bar{F}_h + \Gamma_\pi\bar{F}_e, \\ \tilde{\Delta}_m^e(\theta) &= \bar{\Delta}_m^e(\theta)\eta_m^e = \Delta_e(\theta) + \Gamma_0\bar{F}_e + \Gamma_\pi\bar{F}_h. \end{aligned} \tag{5}$$

In Eq. (5), expressions for $\bar{\Delta}_m^h$ and $\bar{\Delta}_m^e$ can be written with the help of η_m^h and η_m^e that are the renormalization factors for hole and electron pockets and introduce $\bar{\Delta}_h = -\bar{\Delta}_m^e$ and $\bar{\Delta}_m^e(\theta) = \bar{\Delta}_m^e \pm \bar{\Delta}_m^{\bar{e}}\cos(2\theta)$. Then, the first two *Gorkov equations* can be written as

$$\begin{aligned} (i\tilde{\omega}_m^h - \xi_h)G_h + \tilde{\Delta}_h F_h^\dagger \quad &= 1, \\ (i\tilde{\omega}_m^e - \xi_e)G_e + \tilde{\Delta}_e(\theta)F_e^\dagger &= 1 \end{aligned}$$

where

$$G_e = \frac{i\tilde{\omega}_m^e + \xi_e}{(\tilde{\omega}_m^e)^2 + \xi_e^2 + |\tilde{\Delta}_m^e(\theta)|^2}, \quad G_h = \frac{i\tilde{\omega}_m^h + \xi_h}{(\tilde{\omega}_m^h)^2 + \xi_h^2 + |\tilde{\Delta}_m^h|^2}$$

are the normal Green's function for the electron and hole bands. Substituting G_h and G_e in Eq. (4) we find

$$\eta_m^h = 1 + \Gamma_0\frac{1}{\sqrt{(\omega_m^h)^2 + |\bar{\Delta}_m^h|^2}} + \Gamma_\pi\left\langle\frac{1}{\sqrt{(\omega_m^e)^2 + |\bar{\Delta}_m^e(\theta)|^2}}\right\rangle_\theta \tag{6}$$

and $\langle\cdot\rangle_\theta = \frac{1}{2\pi}\int_0^{2\pi} d\theta$ is the average with respect to the angle θ. In a similar way one obtains η_m^e

$$\eta_m^e = 1 + \Gamma_0\left\langle\frac{1}{\sqrt{(\omega_m^e)^2 + |\bar{\Delta}_m^e(\theta)|^2}}\right\rangle_\theta + \Gamma_\pi\frac{1}{\sqrt{(\omega_m^h)^2 + |\bar{\Delta}_m^h|^2}}. \tag{7}$$

Next, one derives in a similar fashion a set of self-consistent gap equations

$$\begin{aligned} \bar{\Delta}_m^h &= \Delta_h - \Gamma_\pi(\bar{\Delta}_m^h - \bar{\Delta}_m^e)\left\langle\frac{1}{\sqrt{\omega_m^2 + |\bar{\Delta}_m^e(\theta)|^2}}\right\rangle_\theta, \\ \bar{\Delta}_m^e &= \Delta_e - \Gamma_\pi(\bar{\Delta}_m^e - \bar{\Delta}_m^h)\frac{1}{\sqrt{\omega_m^2 + |\bar{\Delta}_m^h|^2}}, \\ \bar{\Delta}_m^{\bar{e}} &= \Delta_{\bar{e}} - \Gamma_\pi\bar{\Delta}_m^{\bar{e}}\frac{1}{\sqrt{\omega_m^2 + |\bar{\Delta}_m^h|^2}} - \Gamma_0\bar{\Delta}_m^{\bar{e}}\left\langle\frac{1}{\sqrt{\omega_m^2 + |\bar{\Delta}_m^e(\theta)|^2}}\right\rangle_\theta. \end{aligned} \tag{8}$$

Note that the equations for the bare superconducting gaps in the clean case without impurities Δ_h, Δ_e and $\Delta_{\bar{e}}$ are given by

$$\begin{aligned}
\Delta_h =& -\pi T \sum_{\omega_m}^{\Lambda} \Bigg[\sum_{k',\theta'}^{|\xi_h(k')|<\omega_D} \frac{2U_{hh}\bar{\Delta}^h_m}{\omega_m^2+\xi_h(k')^2+|\bar{\Delta}^h_m|^2} \\
&+ \sum_{k',\theta'}^{|\xi_e(k')|<\omega_D} \frac{2U_{he}\bar{\Delta}^e_m + 4U_{he}\alpha_{he}\bar{\Delta}^{\bar{e}}_m \cos^2 2\theta'}{\omega_m^2+\xi_e(k')^2+|\bar{\Delta}^e_m(\theta')|^2} \Bigg], \\
\Delta_e =& -\pi T \sum_{\omega_m}^{\Lambda} \Bigg[\sum_{k',\theta'}^{|\xi_h(k')|<\omega_D} \frac{2U_{he}\bar{\Delta}^h_m}{\omega_m^2+\xi_h(k')^2+|\bar{\Delta}^h_m|^2} \\
&+ \sum_{k',\theta'}^{|\xi_e(k')|<\omega_D} \frac{2U_{ee}\bar{\Delta}^e_m + 4U_{ee}\alpha_{ee}\bar{\Delta}^{\bar{e}}_m \cos^2 2\theta'}{\omega_m^2+\xi_e(k')^2+|\bar{\Delta}^e_m(\theta')|^2} \Bigg], \\
\Delta_{\bar{e}} =& -\pi T \sum_{\omega_m}^{\Lambda} \Bigg[\sum_{k',\theta'}^{|\xi_h(k')|<\omega_D} \frac{4U_{he}\alpha_{he}\bar{\Delta}^h_m}{\omega_m^2+\xi_h(k')^2+|\bar{\Delta}^h_m|^2} \\
&+ \sum_{k',\theta'}^{|\xi_e(k')|<\omega_D} \frac{4U_{ee}\alpha_{ee}\bar{\Delta}^e_m + 8U_{ee}\beta_{ee}\bar{\Delta}^{\bar{e}}_m \cos^2 2\theta'}{\omega_m^2+\xi_e(k')^2+|\bar{\Delta}^e_m(\theta')|^2} \Bigg].
\end{aligned} \tag{9}$$

These equations hold for two equivalent hole pockets at the Gamma point at $k=(0,0)$ and for two circular symmetry related electron pockets at the X and Y point at $q_1=(\pi,0)$ and $q_2=(0,\pi)$. The intra- and inter-pocket interactions assumed here have the usual form[17]

$$\begin{aligned}
U_{hh_{1,2}}(\phi,\phi') &= U_{hh}, \\
U_{he_{1,2}}(\phi,\theta') &= U_{he}(1\pm 2\alpha_{he}\cos 2\theta'), \\
U_{e_ie_i}(\theta,\theta') &= U_{ee}(1\pm 2\alpha_{ee}(\cos 2\theta+\cos 2\theta')+4\beta_{ee}\cos 2\theta\cos 2\theta'), \\
U_{e_1e_2,e_2e_1}(\theta,\theta') &= U_{ee}(1\pm 2\alpha_{ee}(\cos 2\theta-\cos 2\theta')-4\beta_{ee}\cos 2\theta\cos 2\theta')
\end{aligned} \tag{10}$$

and the $s^{\pm}$ solution is guaranteed for $U_{he}^2 > U_{hh}U_{ee}$. We further assume that the angular dependence of the gap on the electron pockets is not strong enough to produce accidental nodes as, experimentally, there is no evidence for them in $LaFeAsO_{1-x}F_x$. The London penetration depth $\lambda(T)$ scales as $1/\sqrt{\rho_s(T)}$, where $\rho_s(T)$ is the superfluid density. The latter is, up to a factor, the zero frequency value of the current-current correlation function and can be written in the following form for the $s^{\pm}$ superconductor

$$\frac{\rho_s(T)}{\rho_{s0}} = \frac{\pi T}{2}\sum_{\omega_m}\frac{|\bar{\Delta}^h_m|^2}{\eta^h_m(\omega_m^2+|\bar{\Delta}^h_m|^2)^{3/2}} + \left\langle \frac{|\bar{\Delta}^e_m|^2}{\eta^e_m(\omega_m^2+|\bar{\Delta}^e_m(\theta)|^2)^{3/2}} \right\rangle_\theta . \tag{11}$$

* E-mail: g.prando@ifw-dresden.de

[1] A. Kondrat, J. E. Hamann-Borrero, N. Leps, M. Kosmala, O. Schumann, A. Köhler, J. Werner, G. Behr, M. Braden, R. Klingeler, B. Büchner, C. Hess, *Eur. Phys. J.* **B 70**, 461 (2009)

[2] Y. Kamihara, T. Watanabe, M. Hirano, H. Hosono, *Journ. Am. Chem. Soc.* **130**, 3296 (2008)

[3] S. J. Blundell, *Contemp. Phys.* **40**, 175 (1999)

[4] A. Yaouanc, P. Dalmas de Réotier, *Muon Spin Rotation, Relaxation, and Resonance: Applications to Condensed Matter*, Oxford University Press, Oxford (2011)

[5] D. R. Harshman, G. Aeppli, E. J. Ansaldo, B. Batlogg, J. H. Brewer, J. F. Carolan, R. J. Cava, M. Celio, A. C. D. Chaklader, W. N. Hardy, S. R. Kreitzman, G. M. Luke, D. R. Noakes, M. Senba, *Phys. Rev. B* **36**, 2386 (1987)

[6] E. H. Brandt, *Phys. Rev. B* **37**, 2349 (1988)

[7] B. Pümpin, H. Keller, W. Kündig, W. Odermatt, I. M. Savic, J. W. Schneider, E. Kaldis, S. Rusiecki, Y. Maeno, C. Rossel, *Phys. Rev. B* **42**, 8019 (1990)

[8] J. E. Sonier, R. F. Kiefl, J. H. Brewer, D. A. Bonn, J. F. Carolan, K. H. Chow, P. Dosanjh, W. N. Hardy, R. Liang, W. A. MacFarlane, P. Mendels, G. D. Morris, T. M. Riseman, J. W. Scheider, *Phys. Rev. Lett.* **72**, 744 (1994)

[9] J. E. Sonier, J. H. Brewer, R. F. Kiefl, *Rev. Mod. Phys.* **72**, 769 (2000)

[10] P. Carretta, R. De Renzi, G. Prando, S. Sanna, *Phys. Scr.* **88**, 068504 (2013)
[11] H. Luetkens, H.-H. Klauss, R. Khasanov, A. Amato, R. Klingeler, I. Hellmann, N. Leps, A. Kondrat, C. Hess, A. Köhler, G. Behr, J. Werner, B. Büchner, *Phys. Rev. Lett.* **101**, 097009 (2008)
[12] K. Yokogawa, K. Murata, H. Yoshino, S. Aoyama, *Jpn. J. Appl. Phys.* **46**, 3636 (2007)
[13] R. Khasanov, S. Sanna, G. Prando, Z. Shermadini, M. Bendele, A. Amato, P. Carretta, R. De Renzi, J. Karpinski, S. Katrych, H. Luetkens, N. D. Zhigadlo, *Phys. Rev. B* **84**, 100501(R) (2011)
[14] A. Maisuradze, A. Shengelaya, A. Amato, E. Pomjakushina, H. Keller, *Phys. Rev. B* **84**, 184523 (2011)
[15] P. L. Alireza, G. G. Lonzarich, *Rev. Sci. Instr.* **80**, 023906 (2009)
[16] A. B. Vorontsov, M. G. Vavilov, A. V. Chubukov, *Phys. Rev. B* **79**, 140507 (2009)
[17] S. Maiti, M. M. Korshunov, T. A. Maier, P. J. Hirschfeld, A. V. Chubukov, *Phys. Rev. Lett.* **107**, 147002 (2011)